Polymer 49 (2008) 4000–4008

Contents lists available at ScienceDirect

Polymer

journal homepage: www.elsevier.com/locate/polymer

Electrical properties of a composite comprising epoxy resin and α-hematite nanorods

Duško Dudić, Milena Marinović-Cincović, Jovan M. Nedeljković, Vladimir Djoković*

Vinča Institute of Nuclear Sciences, P.O. Box 522, 11001 Belgrade, Serbia

ARTICLE INFO

Article history:
Received 21 February 2008
Received in revised form 16 June 2008
Accepted 7 July 2008
Available online 18 July 2008

Keywords:
Epoxy
Nanocomposite
Dielectric

ABSTRACT

Electrical properties of pure epoxy and epoxy–hematite nanorod composites have been investigated. The nanorods were synthesized by the forced hydrolysis method and further mixed with epoxy to obtain the nanocomposite. TEM analysis revealed that they have an average diameter of about 8 nm, with an average aspect ratio of 25. DC-conductivity and DC-current relaxation measurements showed a significant influence of Fe_2O_3 nanorods on the DC-electrical properties of the epoxy matrix. However, the observed effects of the filler below and above the glass transition are different. Because of their high specific surfaces, nanorods affected segmental mobility of epoxy molecules to a large extent, which resulted in an increase in the glass transition temperature (T_g) and a decrease in the real part of dielectric permittivity in high frequency/low temperature region. It is further observed that at elevated temperatures (above T_g) and low frequencies the real part of dielectric permittivity of the nanocomposite exceeds that of the pure matrix, i.e. there is a transition towards microcomposite-like dielectric behaviour.

1. Introduction

Nanostructured semiconductor–polymer hybrids have been intensively studied in the last two decades because they provide opportunities for preparation of novel high-performance materials that exploit the synergism of the characteristic physical properties of both components [1–4]. However, only recently attention has been paid to possible applications of these nanocomposites as dielectric materials [5–10]. It was suggested that using nano-dielectric fillers in polymers can be beneficiary in terms of improved discharge resistance, dielectric strength, thermal and electric conductivity, etc. Furthermore, because of high specific surface of nanoparticles, they can affect the polymer matrix to a large extent even at quite low weight contents. In this way, it is possible to obtain a material with better mechanical and thermal properties while saving electrical insulation properties of the matrix. Following these current trends, the present investigations are focused on the electrical properties of the composites of epoxy resin and α-hematite nanorods.

α-Hematite (Fe_2O_3) is a semiconductor that absorbs in the visible part of electromagnetic spectrum $E_g = 2.1$ eV. It is non-toxic, environmentally friendly material that is used as a pigment [11], a component of the anti-corrosive coatings [12], a photo- and ordinary-catalyst [13–15]. In our previous studies, a method for incorporating α-Fe_2O_3 nanoparticles into a polystyrene matrix was introduced [16,17]. The characterization of the obtained nanocomposite films revealed a strong influence of the nanoparticles on the thermal stability, the glass transition temperature and the viscoelastic properties of the host polymer. Here, we present a procedure for synthesis of α-Fe_2O_3 nanorods, which are further used as a filler for the epoxy resin. One-dimensional (1D) hematite nanostructures, such as nanowires, nanobelts and nanorods, have been the subject of a number of recent investigations [18–20]. Most of these studies concern the characterization of their structural and optical properties. However, 1D nanoparticles, because of their large specific surfaces, can also be regarded as an ideal choice for the preparation of nanocomposite materials. For this reason, as well as for the reasons mentioned above, we decided to introduce hematite nanorods into the epoxy matrix and to investigate the electrical properties of the obtained nanocomposite. In the first part of the study structural characterization of the hematite nanorods was carried out. In the second part, the influences of several parameters, such as temperature, electric field and accelerated ageing on the electric and dielectric properties of the epoxy film before and after inclusion of nanorods were investigated.

2. Materials and methods

2.1. Sample preparation

2.1.1. Preparation of hematite (α-Fe_2O_3) nanorods

Dispersions of α-Fe_2O_3 nanorods were prepared by "forced hydrolysis", i.e. thermal hydrolysis of iron(III) chloride solution,

* Corresponding author. Tel.: +381 112453986; fax: +381 113440100.
E-mail address: djokovic@vin.bg.ac.yu (V. Djoković).

0032-3861/$ – see front matter © 2008 Elsevier Ltd. All rights reserved.
doi:10.1016/j.polymer.2008.07.016

similar to the method described in the literature [21]. Hundred milliliters of 5.4 M NaOH were added to 100 ml 2 M $FeCl_3$ and the solution was stirred at room temperature for 15 min. After that, the solution was heated up to 100 °C and kept at that temperature for 8 days. The α-Fe_2O_3 nanorods were recovered by centrifugation at 3000 rpm for 15 min, washed out several times with water and dried in vacuum.

2.1.2. Preparation of epoxy–hematite nanocomposites

In order to prepare the nanocomposites, a desired amount of previously synthesized hematite nanorods was immersed into diglycidyl ether of bisphenol-A (DGEBA) prepolymer. The mixture is sonicated for 3 h in order to get a uniform dispersion of the nanorods within the resin. After that, the curing agent aminomethyl 3,3,5-trimethylcyclohexylamin was added with continuous stirring (the epoxy-curing agent ratio was 3:1 by weight). Before they were taken out from the mold, all samples were postcured at 110 °C for 10 min in air. Finally, the mixture was cast into a flat glass mold and outgassed overnight. The obtained planar composite samples had an approximate thickness of 1 mm. Because of the high aspect ratio of the nanorods, the content of the inorganic phase in the composite was chosen to be 2 wt.%. It should be noted that the mixing of the resin and the nanorods was done in strictly controlled conditions but, at the end, we could not prevent a certain particle agglomeration. Pure epoxy plates were prepared in the same way.

2.1.3. Accelerated ageing

In order to investigate the effects of accelerated ageing on the electrical properties of pure epoxy and epoxy–hematite nanorods composites, the samples prepared above were further aged up to 270 h in an Emmerson single vessel oxygen apparatus at 90 °C and 5 MPa oxygen pressure.

2.2. Apparatus

Microstructural characterization of α-Fe_2O_3 nanorods was performed on a Philips EM-400 transmission electron microscope (TEM) operating at 100 kV. The samples for microscopy analysis were deposited on carbon-coated copper grids. The X-ray diffraction (XRD) measurements of α-Fe_2O_3 nanorods were carried out on a Philips PW 1710 diffractometer.

The morphological aspects of the epoxy–hematite interfaces at fracture surfaces were investigated by scanning electron microscopy (Jeol 6460 LV). The samples were fractured after emersion in liquid nitrogen. They were further covered with gold and examined microscopically, at an acceleration voltage of 5 kV.

Differential scanning calorimetry measurements were carried out on a Setaram DSC 151R thermal analyzer in a flowing nitrogen atmosphere. The samples were initially heated from 25 to 127 °C at 10 °C/min, held at this temperature for 1 min to eliminate thermal history effects, and then cooled to 25 °C at 10 °C/min. The reported results are obtained in the second run, using the same experimental conditions.

Electrical DC-conductivity measurements were performed in a shielded cell using Agilent 4339B high resistance meter. Samples were in the form of thin disks 0.9–1 mm thick and about 13 mm in diameter. Electrodes were made on the major faces using silver contact paste. In order to provide the samples the same thermal history, all of them were annealed at 127 °C for 5 min and after that cooled down to room temperature at a rate of 1 °C/min. Prior to measurements, the samples were conditioned for 2 days at a temperature of 23 ± 2 °C in desiccator with humidity of 50 ± 2%. Two types of conductivity measurements were performed:

1. Specific conductivities of the pure epoxy and epoxy–hematite nanocomposite films (aged and as-prepared) were measured as a function of electric field in the range from 0.1 to 2500 V cm^{-1}. Each conductivity value was obtained in 15 s after the application of a certain voltage. Prior to application of the next chosen voltage, the sample was left to relax for another 15 s. To check the effects of electrical ageing, three runs were performed for each sample.
2. The temperature dependences of the specific conductivity of the pure epoxy and the epoxy–hematite nanocomposite films were measured in the range from 20 to 127 °C. The heating and cooling rates were 2 °C/min. A constant current of 2 nA was set during the measurements, with slight variations at the ends of the temperature range because of technical reasons (the resistivity changes during heating and cooling were up to several orders of magnitude).

Agilent 4339B instrument was also used for the measurement of the time dependence of electrical current at a constant voltage of 1000 V cm^{-1}. The measurements were carried out at nine different temperatures: 25, 35, 40, 60, 80, 100, 120, 140 and 160 °C.

Dielectric spectroscopy measurements were performed on an Agilent 4284A instrument in the frequency range between 20 and 10^6 Hz and temperature range from 25 to 152 °C. The preparation, the shape and the conditioning of the samples were the same.

Both instruments (Agilent 4339B and Agilent 4284A) were calibrated against Keithley 5155 standards (10^8–10^{13} Ω, $\Delta R/\Delta V = -0.03\%/V$) at all voltage ranges.

3. Results and discussion

3.1. Structural and morphological characterization

3.1.1. Structural characterization of (α-Fe_2O_3) nanorods

TEM micrograph of the obtained α-hematite nanorods is shown in Fig. 1(a). The size histogram in Fig. 1(b) shows their average diameter to be 8 nm. With respect to diameter, nanorods exhibit much higher differences in lengths. The aspect ratio goes up to 60 with the average value of about 25 (see the inset in Fig. 1(b)). From Fig. 1(a) it can also be concluded that nanorods have a tendency to array parallel to each other and to form bundle-like aggregates.

XRD spectrum of the nanorods is shown in Fig. 2. The observed peaks correspond to 012, 104, 110 and 024 planes of the hematite α-phase [22]. It should also be noted that, in comparison with the standard powder diffraction pattern of bulk α-Fe_2O_3, there is an increase in the intensity of the 012 peak (relative to 104 diffraction peak), indicating preferential growth of nanorods along this direction.

3.1.2. Morphology of the fracture surfaces

SEM micrographs of the fracture surfaces of the pure epoxy and epoxy–hematite nanocomposite are shown in Fig. 3. There is an apparent difference in the fracture behaviour of the two materials. The fracture surface of the pure epoxy is relatively smooth and featureless while a pronounced roughness was observed in the case of the nanocomposite. On the other hand, the detailed scans of the nanocomposite fracture surfaces did not reveal any apparent micron-sized aggregates of the α-Fe_2O_3 nanorods which suggest that they are well dispersed in the epoxy matrix.

3.2. DC-electrical properties

3.2.1. DC-electrical conductivity

Fig. 4 shows the dependence of specific conductivity of the pure epoxy and the epoxy–hematite nanocomposite (aged and as-prepared) from the applied field. It can be seen that prior to

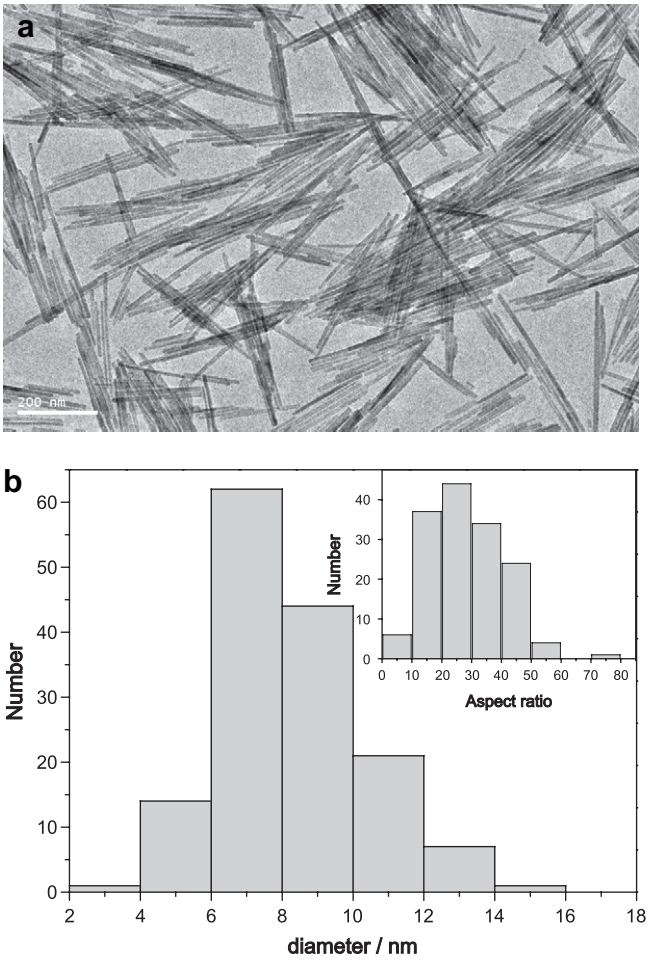

Fig. 1. (a) TEM micrograph of as-prepared α-Fe_2O_3 nanorods. (b) Diameter and aspect ratio (inset) histograms of the nanorods. The number of particles counted for histogram was 150.

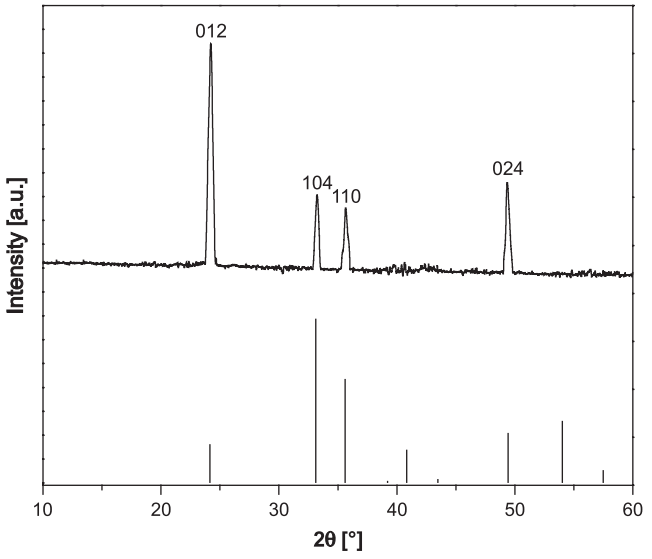

Fig. 2. XRD spectra of nanorod powder (above) and the line spectrum of bulk α-Fe_2O_3 (below).

accelerated ageing the conductivities of the pure epoxy and the nanocomposite films gradually increase with increasing of the electric field. However, in the case of the nanocomposite, the conductivity changes are more pronounced. Obviously, there is a certain contribution of the charge carriers from the filler to the conductivity of the material. Both materials are quite stable with respect to electrical ageing, i.e. there are no significant changes in the conductivity values (of one specific field) after the second and the third run. It can also be noticed in Fig. 4 that accelerated (oxidative) ageing induces an increase in the specific conductivity of the pure epoxy as well as of the nanocomposite. However, the conductivity of the aged nanocomposite film is less dependent on the previous charging history. This implies that the nanostructured hematite can improve to a certain extent the long-term stability of the epoxy with respect to repetitive application of electric field.

The specific conductivity changes of the pure epoxy and the epoxy–hematite nanocomposite during the heating-cooling cycle are shown in Fig. 5(a). Although both materials exhibit conductivity hysteresis, a slightly different behaviour below and above the glass transition temperature (∼50–60 °C) can be noticed (the influence of the nanorods on the glass transition temperature of the matrix will be discussed further in the text). Up to the glass transition temperature, the magnitude of changes of the specific conductivity of the pure epoxy is much higher than that of the nanocomposite, while an opposite effect can be observed after the materials begin to soften (Fig. 5(a)). Eventually, in the investigated temperature range, overall conductivity changes of about five orders of magnitude are noticed for both materials. After their accelerated ageing, this trend is more or less preserved, as it can be seen in Fig. 5(b). However, the differences in the conductivity hystereses of the two films are less pronounced. It should be noted that the results in Fig. 5 suggest that below the softening point the matrix contributes more to the overall conductivity of the nanocomposite. A slower increase in the DC conductivity of the nanocomposite could be explained by the lower mobility of the epoxy segments in the presence of high specific surface fillers. Nevertheless, the change in the curing conditions, probably due to an increased proportion of hardener in the vicinity of nanorod surfaces [5], could also contribute to the observed DC-conductivity behaviour of the nanocomposite. In order to check this assumption, DSC measurements of the pure epoxy and the epoxy–hematite nanocomposites were performed. DSC heating curves of the two materials are shown in Fig. 6. It can be seen that the DSC heat capacity curve of the pure epoxy exhibits a typical glass transition shoulder with the glass transition temperature (taken as the onset of the slope) of about 48 °C. On the other hand, the heat capacity curve of the nanocomposite is smooth, showing no apparent phase transitions in the temperature range investigated here. This result has been checked on several different samples. The softening transition of the nanocomposite is obviously too broad to be observed, which could be the result of the change in the conformation of the epoxy segments close to the surface of nanofiller. For this reason, we decided to estimate the glass transition temperature of the pure epoxy and the epoxy–α-Fe_2O_3 nanocomposite indirectly, using a modified empirical Vogel–Tammann–Fulcher–Hesse (VTFH) equation [23]:

$$\sigma_{DC} = \sigma_{DC0} \exp\left[-\frac{DT_0}{T - T_0}\right], \quad (1)$$

where σ_{DC0}, D and T_0 are fitting parameters. The VTFH equation describes well the dependence of the specific conductivity as well as the dipole relaxation times on the reciprocal temperature in the regions close to the glass transition. Therefore, by fitting experimental results in Fig. 5 to Eq. (1) it is possible to obtain parameters T_0 (the so-called Vogel temperature) and D (strength parameter) which are related to the glass transition temperature, T_g, by the following empirical expression [24,25]:

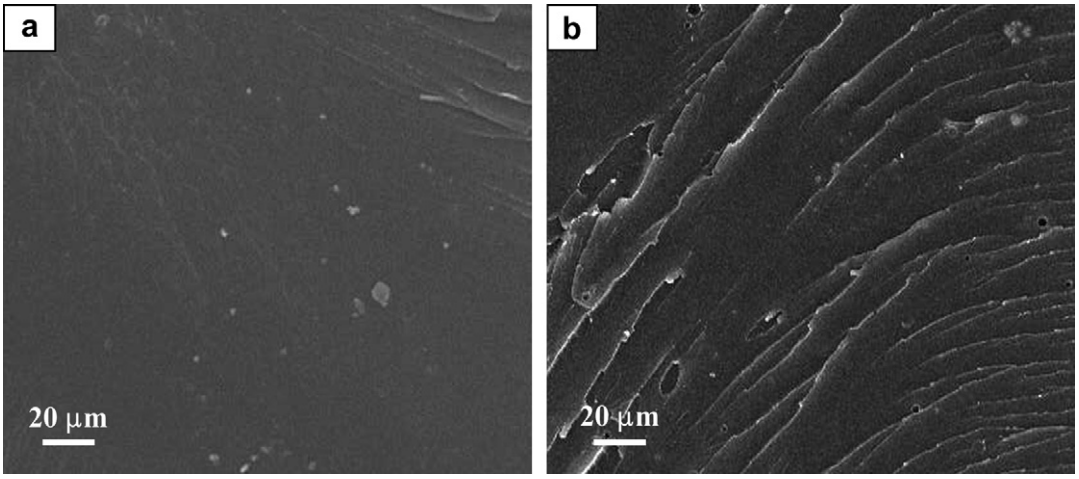

Fig. 3. SEM micrographs of the fracture surface of (a) pure epoxy and (b) epoxy–hematite nanorod composite.

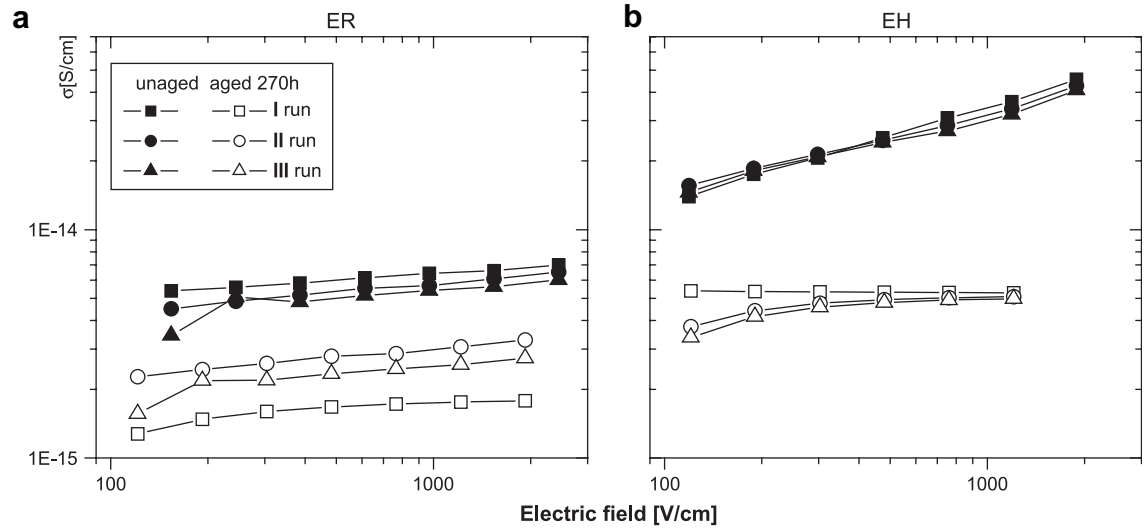

Fig. 4. The DC-conductivity dependence of (a) the pure epoxy and (b) the epoxy–hematite nanorod composite on the applied electric field. The full symbols and the open symbols represent the obtained conductivity values for the unaged and aged (270 h) samples, respectively.

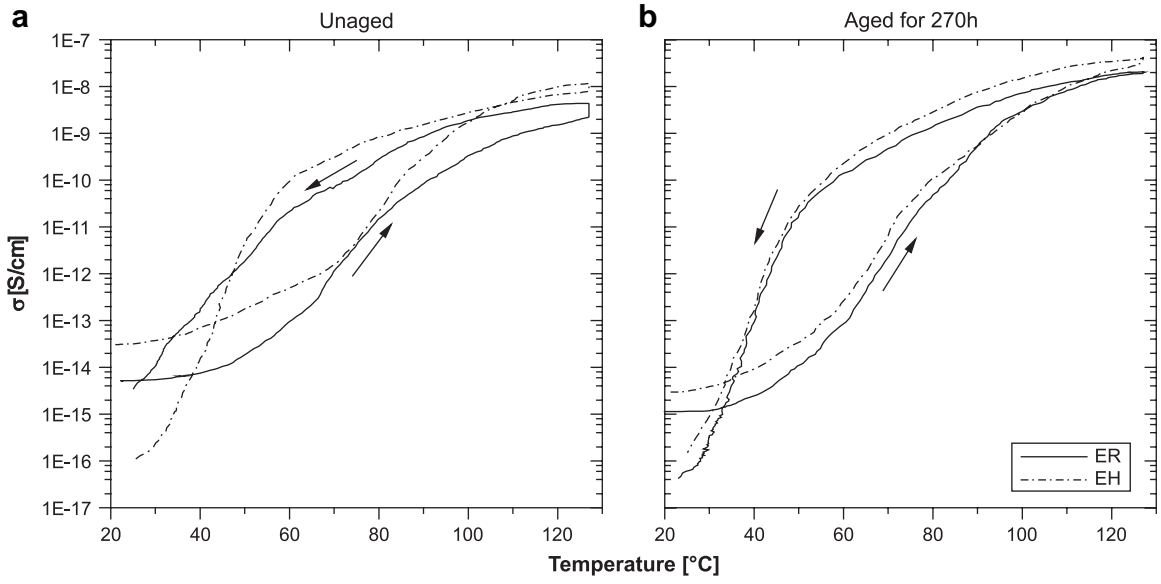

Fig. 5. The DC-conductivity dependence of the pure epoxy and the epoxy–hematite nanorod composite on temperature (a) before and (b) after 270 h of accelerated ageing.

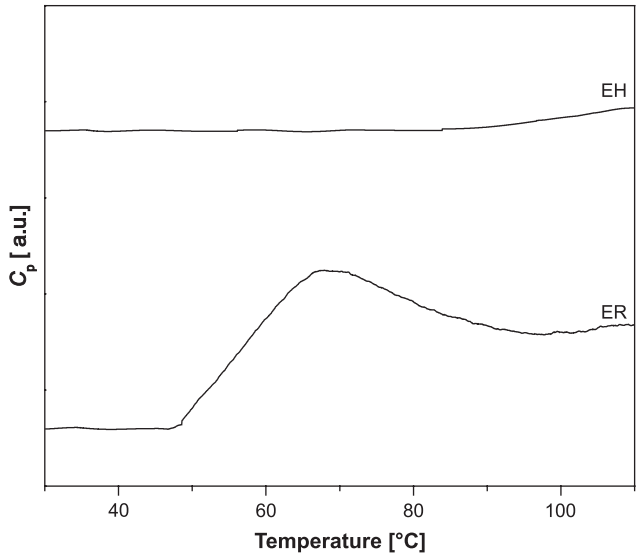

Fig. 6. DSC heat capacity curves of the pure epoxy (ER) and epoxy–α-Fe_2O_3 nanocomposite (EH).

$$T_g = T_0(1 + 0.0255D). \quad (2)$$

Fig. 7 shows the dependences of specific conductivity on the reciprocal temperature for unaged samples (from Fig. 5(a)), while the fits to Eq. (1) are given by the solid lines. The obtained fitting parameters and the corresponding glass transition temperatures estimated through Eq. (2) of all four samples (unaged and aged) are presented in Table 1. In the case of the unaged samples, the results in Table 1 show that the glass transition of the epoxy matrix in the presence of α-Fe_2O_3 nanorods is shifted by 9° towards higher temperature compared to pure epoxy (from 47 to 56 °C). This means that α-Fe_2O_3 nanoparticles indeed reduce the mobility of the matrix bellow the softening point and consequently slow down the conductivity increase with increasing temperature observed in Fig. 5(a). In Table 1 it can further be noticed that the accelerated ageing induces an increase in the glass transition temperature of the pure epoxy and the nanocomposite. However, since the difference in the transition temperatures is similar to that of the unaged samples, the ageing obviously does not significantly affect the interaction of the matrix and the nanorods. Regarding the faster increase of the specific conductivity of the nanocomposite above the softening point, it is probably a result of an easier orientation of the matrix segments (dipoles). This effect can facilitate the transfer of a certain number of the charge carriers introduced by the filler, which in turn gives rise to the overall conductivity. As it will be seen bellow, the DC-current relaxation behaviour is also affected by the change in the mobility of the matrix segments in the presence of α-hematite nanorods.

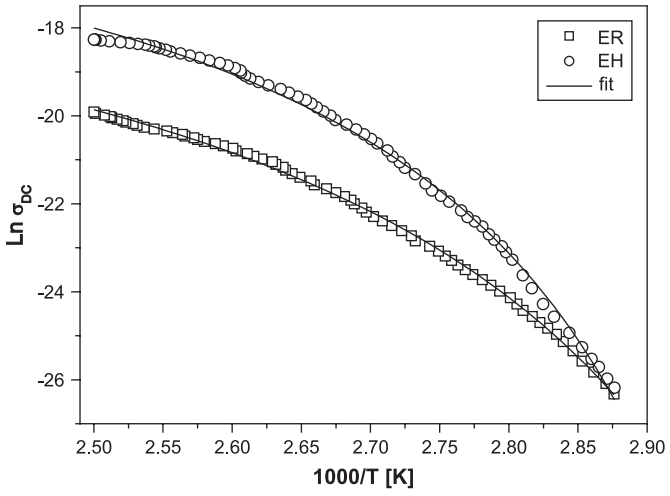

Fig. 7. Dependence of ln σ_{DC} on the reciprocal temperature for the pure epoxy and epoxy–α-Fe_2O_3 nanocomposite. The fit to Eq. (1) is shown by solid line.

3.2.2. DC-current relaxation

Fig. 8 shows DC current vs. time plots of the pure epoxy and the epoxy–α-Fe_2O_3 nanocomposite obtained at different temperatures. At room temperature (25 °C), both materials exhibit a typical DC-current relaxation behaviour. The DC current gradually decreases with time (Fig. 8). This is in agreement with the results of Tuncer et al. [8] on the pure epoxy and the barium titanate filled epoxy resin. However, at higher temperatures there is a change in the current functional dependence on time. After the initial decrease, the current starts to increase and exhibits a weak peak at longer times (~1000 s). In line with the reduced segmental dynamics observed after the introduction of α-Fe_2O_3 nanorods, this effect is observed at 40 °C in the case of the nanocomposite, while the pure matrix shows the same effect at 35 °C. Fig. 8 also shows that at intermediate temperatures (60, 80 and 100 °C) the relaxation curves of the nanocomposite have slightly different shapes than those of the base resin, which should also be attributed to the presence of α-Fe_2O_3 nanorods. Note that there is a change in the magnitude of the specific current as the measurement temperature increases. The nanocomposite shows higher values of the specific current above 100 °C, which is in agreement with its higher values of the specific conductivity observed in Fig. 5(a).

3.3. Dielectric properties

Fig. 9(a) shows the real part of dielectric permittivity of the pure epoxy as a function of frequency and temperature. It can be seen that at low frequencies ε' increases with increasing temperature. An apparent step in ε' values can be noticed at 10^2–10^3 Hz and at temperatures above 80 °C. In this frequency/temperature region dielectric properties are largely controlled by charge transfer processes (the conductivity relaxation and the space charge polarization) [9,10,26]. The dielectric loss results ($\varepsilon'' = \varphi(f, T)$) of the pure epoxy in Fig. 9(b) support the former conclusion. In the low frequency/high temperature regions there is a linear dependence of log ε'' from log f with a slope close to −1 (linear regression in the

Table 1
Parameters of Eq. (1) obtained from the curves in Fig. 7

Sample	Unaged				Aged 270 h			
	σ_{DC0} (S cm^{-1})	T_o (K)	D	T_g (°C)	σ_{DC0} (S cm^{-1})	T_o (K)	D	T_g (°C)
ER	8.4×10^{-5}	308.9	1.41	47.0	8.3×10^{-6}	317.9	1.19	54.5
EH	2.9×10^{-5}	320.7	1.07	56.4	2.5×10^{-6}	323.1	0.91	59.5

The glass transition temperatures (T_g) were obtained using Eq. (2).

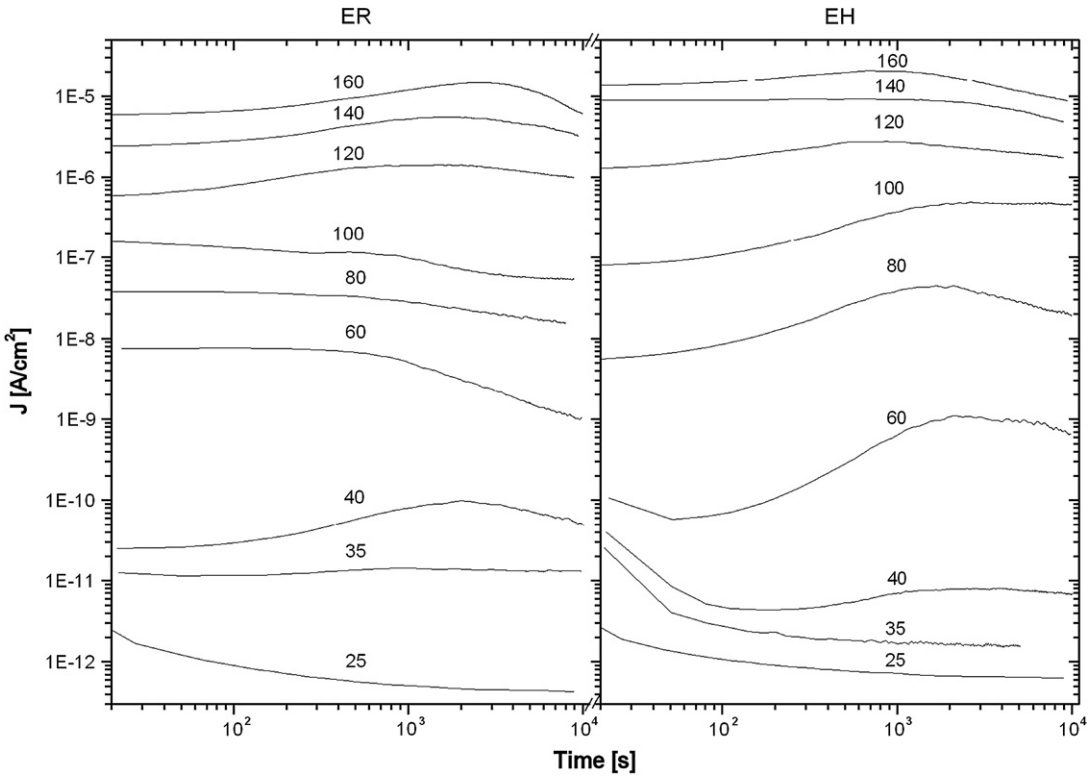

Fig. 8. Current density vs. time relaxation curves of the pure epoxy (ER) and the epoxy–hematite nanorod composite (EH) recorded at different temperatures (25, 35, 40, 60, 80, 100, 120, 140 and 160 °C). During the relaxation measurements the samples are kept at a constant voltage of 1000 V cm^{-1}.

range from 10^1 to 10^3 Hz gives a value of −0.98). In order to illustrate it more clearly, we included $\log \varepsilon'' = \varphi(\log f)$ curves taken at 120, 140 and 152 °C as the inset of Fig. 9(b). The value −0.98 obtained in the linear regression of $\log \varepsilon'' = \varphi(\log f)$ curves is typical for the presence of conductivity current relaxation [27]. According to the model of Yamamoto and Namikawa [28], conductivity current relaxation arises from the accumulation of charges at the interfaces of regions with different conductivity within the bulk of the sample under DC conditions (i.e. at low frequencies). These processes are ensured through charge migration at contact surfaces of the electrodes and the specimen. Taking into account the mentioned model, the data in Fig. 9 suggest that the pure epoxy matrix itself has a highly heterogenic structure.

Real ($\varepsilon' = \varphi(f,T)$) and imaginary ($\varepsilon'' = \varphi(f,T)$) parts of the complex dielectric permittivity of the epoxy–α-Fe_2O_3 nanocomposite are shown in Fig. 10. It can be seen that their functional dependence on frequency/temperature is similar to that of the pure epoxy matrix (Fig. 9). Again, conductivity current relaxations are present in low frequency/high temperature region with a slope $\log \varepsilon'' = \varphi(\log f)$ of −0.98 (see the inset of Fig. 9(b)). It should be noted that in the investigated frequency range the results in Figs. 9 and 10 are in agreement with the results on epoxy–TiO_2 [5], epoxy–silicate [9] and epoxy–diamond [10] nanocomposites. On the other hand, we cannot exclude the presence of interfacial polarization at frequencies below 1 Hz (i.e. outside of the range of the dielectric measurements in this study) observed by Nelson and Fothergill [5]. Also, at the temperature above the glass transition (120 °C), they noticed that pure epoxy exhibits a peak in the loss tangent at 0.1 Hz. At the same time, the epoxy–TiO_2 nanocomposite showed low frequency dispersion or quasi-DC behaviour characterized by flattening of loss tangent at frequencies below 0.1 Hz. Although we did not investigate the dielectric properties in this frequency region, our DC relaxation curves in Fig. 8 could offer some information about previously mentioned low frequency (i.e. long relaxation times) processes. It has already been discussed in Section 3.2.2 that increasing of the temperature leads to the appearance of a peak in the relaxation curves at approximately 10^3 s. Obviously, certain processes are thermally activated at longer times. In order to make the exact comparison between these thermally activated processes and the processes at low frequencies (<0.1 Hz) stated above, it would be necessary to determine their distribution of the relaxation times (τ_i) by spectral analysis of the relaxation curves $J(t)$ in Fig. 8. Tuncer et al. [8] applied non-parametric data inversion method in the analysis of $I(t)$ relaxation curves of the pure epoxy and the epoxy–$BaTiO_3$ nanocomposites recorded at room temperature. From the estimated distributions of the relaxation times they have concluded that there is a difference between the filled and unfilled samples at longer times. The mentioned numerical analysis is out of scope of the present investigation; however, even a simple comparison of $J(t)$ curves in Fig. 8 implies that the long-time processes activated at high temperatures are strongly affected by the presence of α-Fe_2O_3 nanorods.

In Fig. 11 the specific alternating conductivity (σ_{AC}) of epoxy–α-Fe_2O_3 nanocomposite is plotted vs. frequency and temperature. The low frequency/high temperature plateau observed in σ_{AC} (Fig. 11) corresponds to the DC conductivity (σ_{DC}). This plateau of the constant conductivity can actually be related to the linear part of $\log \varepsilon''$ curve at low frequencies (Fig. 10, inset). Further increasing of the frequency (in this high temperature region) leads to a change in the mechanism of electric conduction. The functional dependence of the observed constant σ_{DC} plateau values from the reciprocal temperature can again be described by the VFTH expression (Eq. (1)). Fig. 12 shows the corresponding $\log \sigma_{DC}$ values (taken at 20 Hz) vs. $1/T$ curves of the pure epoxy and the nanocomposite. The parameters obtained by fitting the experimental data to Eq. (1) are given in Table 2. The glass transition temperatures estimated by using Eq. (2) are also included. The obtained T_g values are a

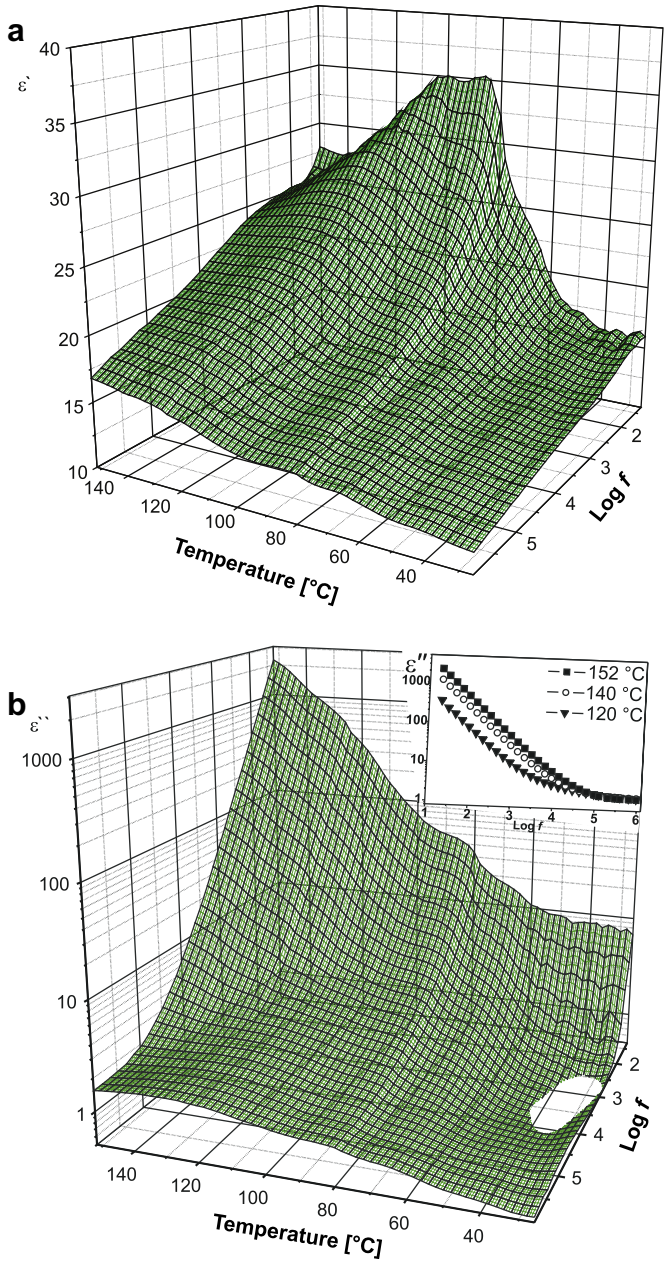

Fig. 9. (a) The real and (b) imaginary parts of dielectric permittivity of the pure epoxy resin as a function of temperature and frequency. Inset: ε'' vs. frequency at 120, 140 and 152 °C.

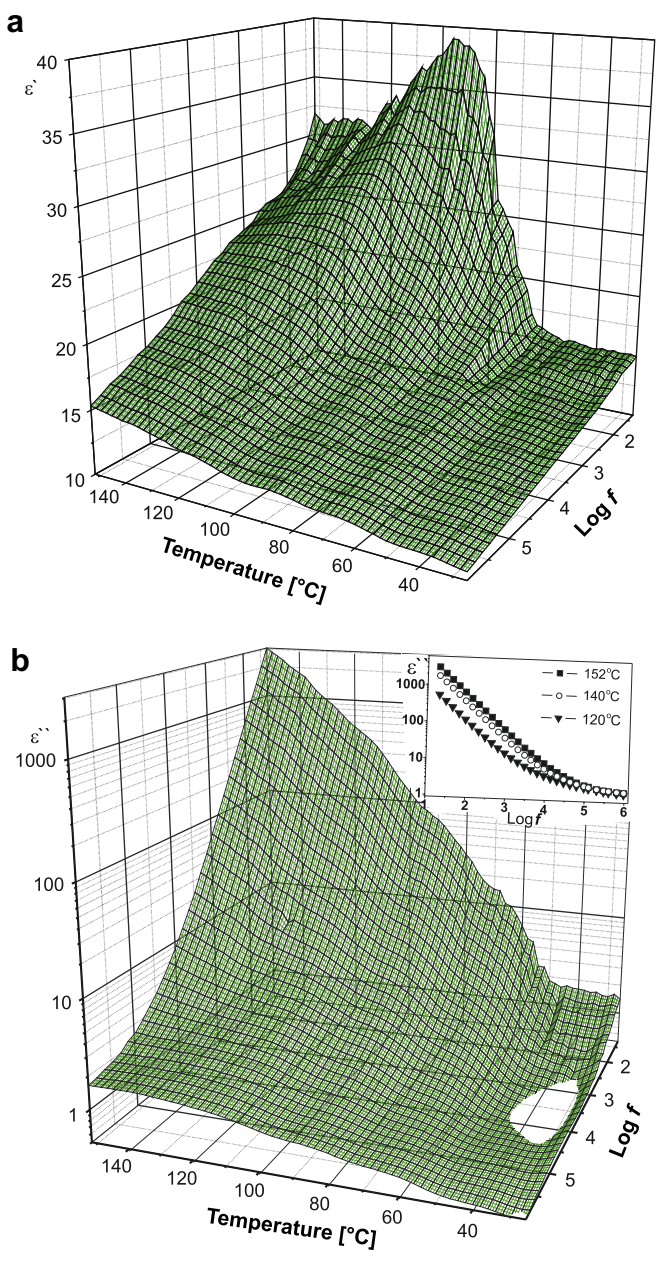

Fig. 10. (a) The real and (b) imaginary parts of dielectric permittivity of the epoxy–α-Fe_2O_3 nanocomposite as a function of temperature and frequency. Inset: ε'' vs. frequency at 120, 140 and 152 °C.

little bit lower than these obtained by direct DC-conductivity measurements, Table 1 (unaged samples). However, in both cases, the estimations gave a similar increase in the glass transition temperature of the epoxy after the introduction of the α-Fe_2O_3 nanorods.

There is another effect that should be emphasized here, which could also be the result of the altered mobility of the matrix segments in the presence of nanorods (suggested by the formerly observed increase in the glass transition temperature). It is the change in the magnitude of the real part of the dielectric permittivity of the epoxy–hematite nanocomposite (ε'_{EH}) with respect to that of the pure epoxy resin (ε'_{ER}). We illustrate this in Fig. 13, where the relative change of dielectric permittivity (defined as $\Delta\varepsilon' = 100(\varepsilon'_{EH} - \varepsilon'_{ER})/\varepsilon'_{ER}$) is plotted vs. frequency and temperature. It can be seen that $\Delta\varepsilon'$ is about −10%, except in the range of temperatures of 100–152 °C and low frequencies. This means that in the low temperature/high frequency regions ε' of the nanocomposite decreases due to reduced segmental mobility of the matrix, induced by α-Fe_2O_3 nanorods. The nanorods immobilize to a certain extent the end-chain and/or the side-chain movement of the epoxy molecules, which influences the molecular polarization and consequently reduces the permittivity of the matrix. Similar effects of the nanofiller on the dielectric permittivity of the epoxy resin have been noticed by several authors/groups [5,8,9,10]. The main difference between the present and the mentioned studies is that the nanocomposite exhibits higher ε' values ($\Delta\varepsilon' \sim 10$–15%) in the high temperature (above 100 °C) and the low frequencies (below 10^2 Hz) region, as it can be seen in Fig. 13. We believe that the main reason for the observed behaviour is the shape of our α-Fe_2O_3 nanofiller. Fig. 1 shows that the nanorods have an average

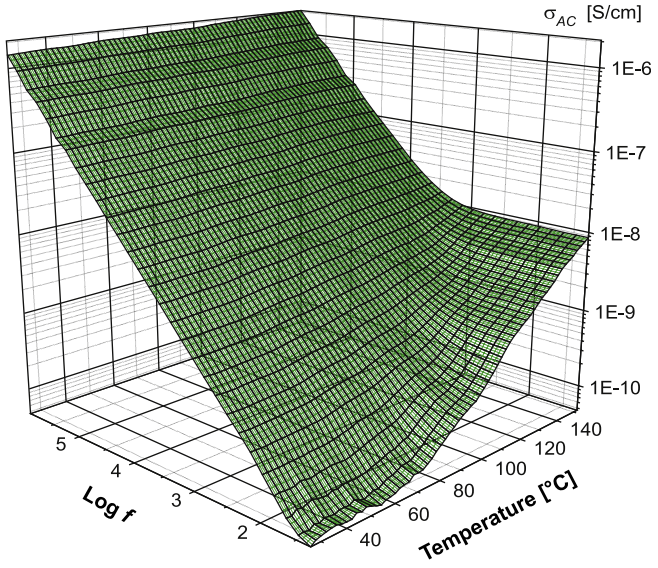

Fig. 11. The specific alternating conductivity (σ_{AC}) of the epoxy–α-Fe_2O_3 nanocomposite as a function of temperature and frequency.

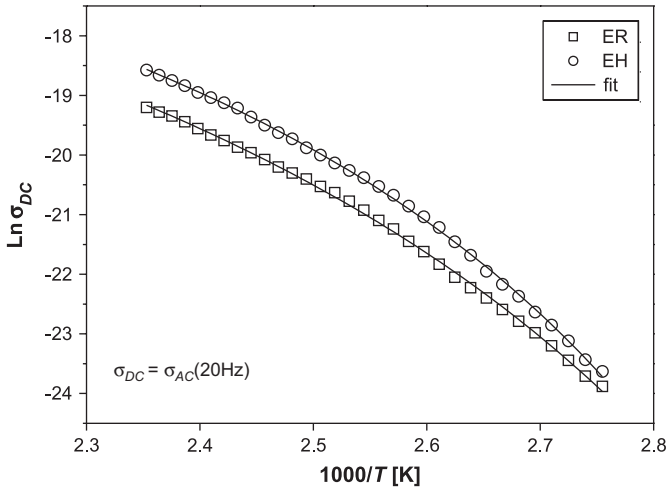

Fig. 12. Dependence of ln σ_{DC}($\sigma_{DC} = \sigma_{AC}$ at 20 Hz) on the reciprocal temperature for the pure epoxy (ER) and epoxy–α-Fe_2O_3 nanocomposite (EH). The fit to Eq. (1) is shown by solid line.

Table 2
Parameters of Eq. (1) obtained from the curves in Fig. 12

Sample	Unaged			
	σ_{DC0} (S cm^{-1})	T_o (K)	D	T_g (°C)
ER	3.3×10^{-5}	288.9	3.55	41.0
EH	4.0×10^{-5}	300.7	2.85	49.1

The glass transition temperatures (T_g) were obtained using Eq. (2).

diameter of about 8 nm but their length is already in sub-micron or micron domain. It seems that above the glass transition temperature (at low frequencies) the geometry factors start to dominate over matrix–nanorod interaction. In other words, α-Fe_2O_3 nanorods start to behave more like micron filler, which, according to the literature, gives rise to dielectric permittivity of the matrix [5].

The conductivity current relaxation and space charge polarization are the dominant effects in the high temperature/low frequency region. In order to investigate the effects of α-Fe_2O_3 nanorods on dipolar polarization process one must examine the results obtained at higher frequencies. Fig. 14 shows the temperature ε'' plots of the pure epoxy and the epoxy α-Fe_2O_3 nanocomposite at a fixed frequency of 960 kHz. In these curves, two characteristic shoulders (at approximately 65 and 80 °C) as well as a peak at ~120 °C can be noticed, which are slightly shifted towards higher temperatures after the introduction of the α-Fe_2O_3 nanorods. In agreement with the glass transition temperature results presented in Tables 1 and 2, the observed shift of ε'' plot confirms the observed effects of nanorods on the segmental mobility, not only in the vicinity of filler particles but also on the material as a whole. On the other hand, the magnitude of the ε'' values in Fig. 14 is much higher than these reported in the literature [9,10], which implies that even at these high frequencies (960 kHz) the contributions of the conductivity relaxation and the space charge polarization cannot be completely neglected.

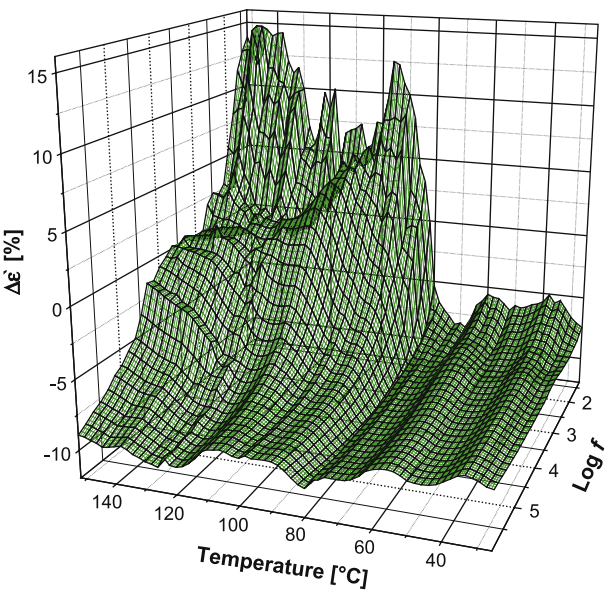

Fig. 13. Relative changes of $\Delta\varepsilon'$ of the real part of dielectric permittivity (defined as $\Delta\varepsilon' = 100(\varepsilon'_{EH} - \varepsilon'_{ER})/\varepsilon'_{ER}$) after the introduction of α-Fe_2O_3 nanorods into epoxy resin (ER).

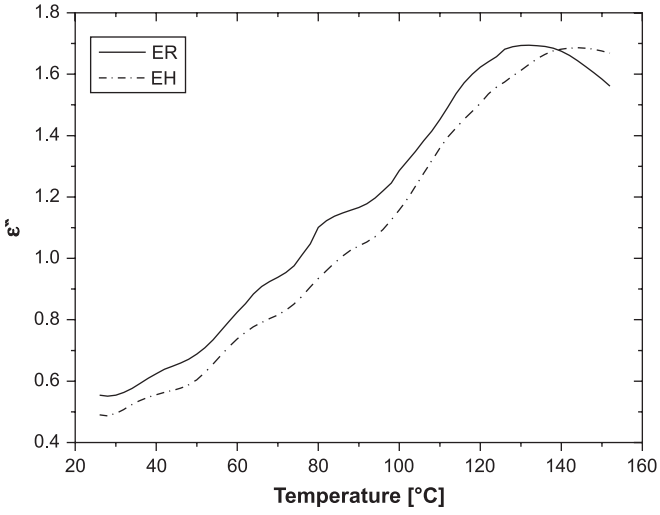

Fig. 14. ε'' vs. temperature plots of the pure epoxy (ER) and the epoxy–α-Fe_2O_3 nanocomposite (EH) at a fixed frequency of 960 kHz.

4. Conclusions

In this paper we investigate the influence of the hematite nanorods on the DC-electric and dielectric properties of the epoxy matrix. The TEM measurements have shown that as-prepared nanorods have an average diameter of about 8 nm and an average aspect ratio of 25. Their XRD spectrum corresponds to α-hematite crystal phase. Significant changes in the DC-conductivity behaviour of the epoxy resin during the heating/cooling cycle were noticed after the inclusion of α-Fe_2O_3 nanorods. The dependence of $\ln \sigma_{DC} = \varphi(1/T)$ was studied in terms of the Vogel–Tammann–Fulcher–Hesse equation. In the fitting procedure, an increase in the nanocomposite glass transition temperature of about 9 °C was found due to restricted segmental mobility of the matrix induced by the filler.

Reduced mobility of the epoxy molecules after the introduction of α-Fe_2O_3 nanorods has a profound effect on the dielectric properties of the matrix. The nanocomposite shows lower values of the real part of the dielectric permittivity in high frequency/low temperatures regions. At temperatures well above the glass transition, ($\sim$100 °C) and at low frequencies ε' of the nanocomposite starts to override ε' of the pure epoxy, i.e. a microfiller-like influence of the nanorods on the dielectric properties of the matrix was observed.

Acknowledgments

This work is financially supported by the Serbian Ministry of Science (grant numbers 141013 and 142066). The authors would like to acknowledge helpful discussions with Prof. Polycarpos Pissis from the National Technical University of Athens. We are also grateful to Dr Natasa Bibic for performing TEM measurements.

References

[1] Balazs AC, Emrick T, Russell TP. Science 2006;314:1107–10.
[2] Huynh WU, Dittmer JJ, Alivisatos AP. Science 2002;295:2425–7.
[3] Godovsky DY. Adv Polym Sci 2000;153:163–205.
[4] Caseri W. Macromol Rapid Commun 2000;21:705–22.
[5] Nelson JK, Fothergill JC. Nanotechnology 2004;15:586–95.
[6] Fréchette MF, Trudeau ML, Alamdari HD, Boily S. IEEE Trans Dielectr Electr Insul 2004;11:808–18.
[7] Nelson JK, Hu Y. J Phys D Appl Phys 2005;38:213–22.
[8] Tuncer E, Sauers I, James DR, Ellis AR, Paranthaman MP, Aytug T, et al. Nanotechnology 2007;18:025703 (6 pp.).
[9] Kanapitsas A, Pissis P, Kotsilkova R. J Non-Cryst Solids 2002;305:204–11.
[10] Pissis P, Fragiadakis D. J Macromol Sci B Phys 2007;46:119–36.
[11] Morse PG. Chem Eng News 1998;76(41):42–62.
[12] Oh SE, Cook DC, Townsend HE. Corros Sci 1999;41:1687–702.
[13] Ohmori T, Takahashi H, Mametsuka H, Suzuki E. Phys Chem Chem Phys 2000;2:3519–22.
[14] Pestman R, Koster RM, Boellaard E, van der Kraan AM, Ponec V. J Catal 1998;174:142–52.
[15] Lin S-S, Gurol MD. Environ Sci Technol 1998;32:1417–23.
[16] Marinović-Cincović M, Šaponjić ZV, Djoković V, Milonjić SK, Nedeljković JM. Polym Degrad Stab 2006;91:313–6.
[17] Djoković V, Nedeljković JM. Macromol Rapid Commun 2000;21:994–7.
[18] Wen X, Wang S, Ding Y, Wang ZL, Yang S. J Phys Chem B 2005;109:215–20.
[19] Vayssieres L, Beermann N, Lindquist SE, Hagfeldt A. Chem Mater 2001;13:233–5.
[20] Raming TP, Winnubst AJA, van Kats CM, Philipse AP. J Colloid Interface Sci 2002;249:346–50.
[21] Matijevic E. Langmuir 1986;2:12–20.
[22] Sadykov VA, Isupova LA, Tsybulya SV, Cherepanova SV, Litvak GS, Burgina EB, et al. J Solid State Chem 1996;123:191–202.
[23] Angell CA. J Non-Cryst Solids 1991;13:131–3.
[24] Polizos G, Shilov VV, Pissis P. Solid State Ionics 2001;145:93–100.
[25] Angell CA. Annu Rev Phys Chem 1992;43:693–717.
[26] Nikonorova NA, Barmatov EB, Pebalk DA, Barmatova MV, Domínguez-Espinosa G, Diaz-Calleja R, et al. J Phys Chem C 2007;111:8451–8.
[27] Hedvig P. Dielectric spectroscopy of polymers. Budapest: Akadémiai Kiadó; 1977.
[28] Yamamoto K, Namikawa H. Jpn J Appl Phys 1988;27:1845–51.